THE JOURNAL OF PHYSICAL CHEMISTRY C

Article

Cite This: J. Phys. Chem. C XXXX, XXX, XXX−XXX

pubs.acs.org/JPCC

Study of the Partial Substitution of Pb by Sn in Cs−Pb−Sn−Br Nanocrystals Owing to Obtaining Stable Nanoparticles with Excellent Optical Properties

Ana Beatriz Ferreira Vitoreti,[†,‡,§] Said Agouram,[∥] Mauricio Solis de la Fuente,[⊥] Vicente Muñoz-Sanjosé,[∥] Marco Antônio Schiavon,[‡] and Iván Mora-Seró*[,†]

[†]Institute of Advanced Materials (INAM), Universitat Jaume I, 12006 Castelló, Spain

[‡]Department of Natural Science, Federal University of São João del-Rei, 36301-160 São João del-Rei, Brazil

[§]CAPES Foundation, Ministry of Education of Brazil, Brasília, 70040-020, Brazil

[∥]Department of Applied Physics and Electromagnetism, University of Valencia, 46100 Valencia, Spain

[⊥]Lawrence Berkeley National Laboratory, Energy Technologies Area, 1 Cyclotron Road, Berkeley, California 94720, United States of America

Supporting Information

ABSTRACT: Halide perovskites are revolutionizing the photovoltaic and optoelectronic fields with outstanding performances obtained in a remarkably short time. However, two major challenges remain: the long-term stability and the Pb content, due to its toxicity. Despite the great effort carried out to substitute the Pb by a less hazardous element, lead-free perovskite still remains more unstable than lead-containing perovskites and presents lower performance as well. In this work, we demonstrate the colloidal preparation of Cs−Pb−Sn−Br nanoparticles (NPs) where Sn is incorporated up to 18.8%. Significantly, we have demonstrated that the partial substitution of Pb by Sn does not produce a deleterious effect in their optical performance in terms of photoluminescence quantum yield (PLQY). We observed for the first time a positive effect in terms of enhancement of PLQY when Sn partially substitutes Pb in a considerable amount (i.e., higher than 5%). PLQYs as high as 73.4% have been obtained with a partial Pb replacement of 7% by Sn. We present a systematic study of the synthesis process in terms of different growth parameters (i.e., precursor concentration, time, and temperature of reaction) and how they influence the Sn incorporation and the PLQY. This high performance and long-term stability is based on a significant stabilization of Sn^{2+} in the NPs for several months, as determined by XPS analysis, and opens an interesting way to obtain less Pb-containing perovskite NPs with excellent optoelectronic properties.

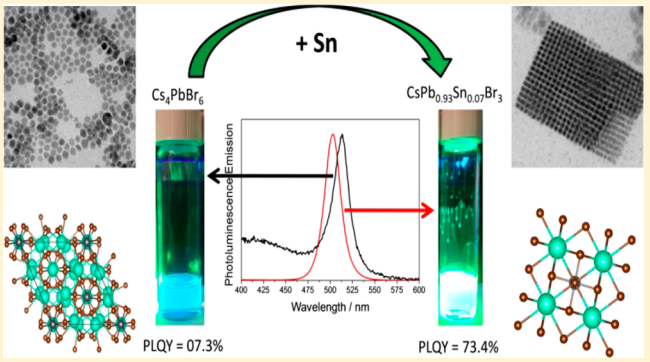

1. INTRODUCTION

In the past few years, the photovoltaic field first and later the optoelectronic field have been shaken by the emergence of a newcomer family of materials: the halide perovskites.[1] Polycrystalline halide perovskite thin film has exhibited photoconversion efficiencies higher than 22%[2] and external quantum emission higher than 10% for perovskite LEDs.[3] These promising results on thin films have pushed the interest up of these materials in nanoparticle form. Colloidal semiconductor nanoparticles (NPs) have attracted intensive studies in the recent decades as future optoelectronic materials[4,5] owing to unique features such as size-dependent emission wavelength, narrow emission spectrum, and high luminescent efficiency.[6,7] Since the seminal work on colloidal organic−inorganic perovskite NPs ($CH_3NH_3PbX_3$, X = Cl, Br, I) synthesized in 2014 by Perez-Prieto and co-workers[8] and on colloidal all-inorganic perovskites ($CsPbX_3$ = X = Cl, Br, I) synthesized by Kovalenko and co-workers in 2015,[9] many works have been published in the past few years,[10−16] including their applications in light-emitting diodes, solar cells, and photodetectors.[17−22] The interest in halide perovskite NPs arises due to their high photoluminescence quantum yields (PLQYs), despite the relatively simple synthesis method,[9] but also by the possibility of stabilizing structures that are nonstable in bulk thin films. Certainly, the most clear example is the stabilization of the cubic phase of $CsPbI_3$ NPs at room temperature, while this phase is not stable at the same

Special Issue: Prashant V. Kamat Festschrift

Received: March 14, 2018
Revised: April 29, 2018
Published: April 29, 2018

DOI: 10.1021/acs.jpcc.8b02499
J. Phys. Chem. C XXXX, XXX, XXX−XXX

temperature in bulk thin films.[23] In fact, the current record efficiency for quantum dot solar cells has been obtained using $CsPbI_3$ NPs.[24]

These antecedents have encouraged us to evaluate the potentiality of the halide perovskite NP system in order to partially replace Pb by a less hazardous element such as Sn. Although perovskite-based photovoltaic and optoelectronic performance is striking the research community, this new technology faces two major challenges: the increase of long-term stability and the reduction of Pb content without a decrease in performance and stability. The Pb toxicity in these perovskite optoelectronics devices hinders its large-scale applications. However, despite the great effort carried out in order to substitute the Pb by a less hazardous element, lead-free perovskite still is more unstable than lead-containing perovskites,[25,26] and presents inferior optoelectronic device performance.[27−30] One alternative to palliate the drawbacks of the total Pb replacement is the partial substitutions owing to reduce the Pb content. There is a great interest in replacing part of the Pb amount by Sn, Bi, Zn, or Mn.[30−34] Recently, impressive photoconversion efficiencies higher than 17% have been obtained for perovskite solar cells where Pb was partially substituted by Sn.[35] However, despite the enormous progress of the efficiencies for less Pb-containing perovskite thin films, their performance is still below the current state-of-the-art of pure-Pb halide perovskites.

The main scope of this work was to investigate if the use of perovskite NPs could relax the perovskite bulk constraints and if the partial substitution of Pb by Sn could be reached without any decrease in terms of the optical properties, i.e., high PLQY and narrow photoluminescence (PL) full width at half-maximum (fwhm). For stability reasons, we have performed the analysis on full inorganic halide perovskite nanoparticles in the system Cs−Pb−Sn−Br. In the case of fully inorganic compounds, starting from almost the same precursors, several synthesis procedures have been reported producing different structures, with different sizes and morphological shapes.[36−38] The main obtained compounds from the combination of Cs and Pb, and by using Br as a halide anion, are $CsPbBr_3$, $CsPb_2Br_5$, and Cs_4PbBr_6, resulting from different synthesis conditions by changing only the precursor amount.[39−42] In this sense, we have investigated the partial substitution of Pb by Sn as a function of the different synthesis parameters, i.e., precursor concentration, temperature, and time reaction. Previous results indicate that the performance of the halide perovskite NPs is severely damaged when Pb is partially substituted by Sn in a substantial amount (>5%). It is the case observed for $CsPb_{1-x}Sn_xI_3$ that exhibits a low PLQY due to the self-doping when Sn oxidizes from Sn^{2+} to Sn^{4+}.[43] On the other hand, it has been reported that the replacement of Pb^{2+} by Sn^{4+} can increase the PLQY of halide perovskite NPs.[44] In that work, the real amount of incorporated Sn^{4+} ions was determined by inductively coupled plasma emission spectroscopy (ICP-AES), presenting a real content of Sn of 0.3%.[44] In fact, there are not previous results in which a substantial amount of Sn is incorporated into halide perovskite NPs, preserving their optical properties in an outstanding way. In this work, we have demonstrated the colloidal preparation of halide perovskite NPs in the system Cs−Pb−Sn−Br, in which Sn is incorporated at a rate of up to 18.8% maintaining a PLQY as high as 65%. We have shown undoubtedly that the synthesis temperature and the ligand amount play an important role in the kind of Cs−Pb−Sn−Br compounds that can be obtained, regarding the size of nanocrystals, their optical properties, and their colloidal stability. PLQYs as high as 73.4% have been obtained with a Sn-replacing rate of 7%. This outstanding performance despite the relative high amount of Sn was attributed, in an important extent, to the significant stabilization of Sn^{2+}, which remains for months in the prepared halide perovskite NPs. For the first time, we observe that the optical properties of halide perovskite NPs, in which Pb has been partially substituted by Sn, surpass the ones observed for similar nanoparticles just containing Pb as the metallic cation.

2. MATERIALS

1-octadece (ODE) 90%, Oleic Acid (OA) 90%, Oleylamine (OLEA) ≥ 98%, Cesium carbonate (Cs_2CO_3) 99.9%, Tin Bromide ($SnBr_2$), Trioctylphosphine (TOP) 90%, Hexane for HPLC ≥ 97.0%, all from Sigma-Aldrich and Lead Bromide ($PbBr_2$) for perovskite precursors from TCI. All of the reagents were used without any purification.

3. METHODS

3.1. Preparation of Cesium-Oleate Solution. Cesium-oleate solution was prepared according to the approach reported by Kovalenko and co-workers.[9] In brief, 0.4 g of Cs_2CO_3, 1.2 mL of OA, and 15 mL of ODE were loaded in a three-neck flask and degassed under a vacuum at 120 °C for 1 h, followed by heating at 150 °C under a N_2 atmosphere until all Cs_2CO_3 reacted with OA.

3.2. Preparation of Cs−Pb−Br Nanoparticles. Cs−Pb−Br nanocrystals was prepared following the approach reported by Liu et al.[45] A 0.054 g portion of $PbBr_2$ and 5 mL of ODE were loaded in a three-neck flask and dried under a vacuum for 1 h at 120 °C. A 2 mL portion of OLEA and 2 mL of OA were injected at 120 °C under N_2. After the complete dissolution of $PbBr_2$, the temperature was increased to 150 °C. Finally, 0.6 mL of hot (150 °C) Cs-oleate solution was quickly injected and the reaction mixture was cooled by ice-bath after 5 s.

3.3. Preparation of Cs−Pb−Sn−Br Nanoparticles. We have adapted the procedure reported by Liu et al.[45] to Sn incorporation on $CsPbBr_3$ nanocrystals. Briefly, $PbBr_2$ and $SnBr_2$ with a specific molar ratio were mixed with 5 mL of ODE and 1 mL of TOP in a three-neck flask and dried under a vacuum for 1 h at 120 °C. A 2 mL portion of OLEA and 2 mL of OA were injected at 120 °C under N_2. After the complete dissolution of $PbBr_2$ and $SnBr_2$, the temperature was increased (130−170 °C). Then, 0.6 mL of hot (150 °C) Cs-oleate solution was quickly injected and the reaction mixture was cooled by ice-bath after 5 s.

3.4. Nanoparticle Washing. Cs−Pb−Br and Cs−Pb−Sn−Br NPs were extracted from the crude solution after synthesis by centrifugation at 4700 rpm for 10 min, and the colored supernatant was discarded. Then, 1 mL of hexane was added and the NPs were dispersed by shaking. Then, the suspension was centrifuged at 4000 rpm for 3 min to precipitate the larger NPs and agglomerates that were discarded. In the supernatant, there were only the NPs dispersed in hexane.

3.5. Characterization. X-ray diffraction (XRD) patterns of all samples were obtained by using a Diffractometer D4 Endeavor from Bruker-AXS using a Cu Kα radiation source (λ = 1.54056 Å). The UV−VIS absorption spectra were recorded on a UV−Visible Spectrophotometer Cary 300 Bio (UV0911M312 Varian). The emission spectra (PL) were taken by using a Horiba Fluorolog 3-11. The absolute PLQY of

DOI: 10.1021/acs.jpcc.8b02499
J. Phys. Chem. C XXXX, XXX, XXX−XXX

the perovskite NPs was determined by using a PLQY Absolute QY Measurement System (C9920-02) equipped with an integrating sphere, with a wavelength excitation of λ_{exc} = 355 nm. Morphological, compositional, and structural analysis of samples was performed by high-resolution transmission electron microscopy (HRTEM) with a field emission gun TECNAI G2 F20 microscope operated at 200 kV, having the capabilities of selected area electron diffraction (SAED) and energy dispersive X-ray spectroscopy (EDX). To prepare the TEM samples, a drop of the perovskite NP solution (10 mg/mL in hexane) was deposited onto carbon film supported on a copper grid, which was subsequently dried. For X-ray photoelectron spectroscopy (XPS), films of NPs were deposited on glass substrates (Corning, 1.5 × 1.5 cm^2) by spin coating (4000 rpm, 60 s), using 20 mg/mL solution in toluene; XPS spectra were obtained using PHI 5400 XPS, Mg Kα X-ray monochromatic source 1253.6 eV line width 0.7 eV, spot size 400 μm. The carbon peak was used as a reference, position peak 1s = 284.5 eV in measurements. All of the measurements were performed at room temperature.

4. RESULTS

The synthesis of halide perovskite NPs in the system Cs−Pb−Sn−Br by the hot injection method has been analyzed as a function of different synthesis parameters with the aim of partially substituting Pb by Sn. The structural analyses of the resulting NPs were carried out by XRD, TEM, and EDX, while the optical properties have been characterized by light absorption, photoluminescence (PL), and PLQY. The main results for the different synthesis parameters such as the reaction temperature, the Pb and Sn precursor rate, and the reaction time are summarized in sections 4.1, 4.2, and 4.3, respectively. Two kinds of halide perovskite NPs have been found under the different synthesis conditions studied, i.e, $CsPbBr_3$ and Cs_4PbBr_6, as determined by XRD. Despite that part of the Pb has been substituted by Sn, we preferred to use these formula names in the manuscript, highlighting in which percentage Pb has been partially substituted by Sn, to avoid long and confusing names including Pb and Sn.

4.1. Reaction Temperature. The reaction temperature plays a key role during the synthesis process determining in a broad extent the nature of the NPs obtained as well as the dimensionality and size of the colloidal perovskite nanocrystals.[46,47] The effect of this parameter has been analyzed keeping precursors and ligand concentrations constant as well as the reaction time, 5 s, and changing just the reaction temperature from 130 to 170 °C; see Table 1. The obtained solutions after each synthesis have been systematically characterized by XRD, absorption and emission spectroscopies and TEM; see Figure 1. The observed diffraction peaks with XRD, see Figure 1a, present a good agreement with the peaks of Cs_4PbBr_6 tetragonal structure (ICDS 162158) and cubic perovskite $CsPbBr_3$ structure (ICDS 109295), bottom of Figure 1a. Both crystalline structures are represented in Figure S1a,b. However, the exact determination of the $CsPbBr_3$ crystalline phase is not straightforward, as cubic and orthorhombic phases present close diffraction peaks. While first reports pointed to a cubic phase,[48] more accurate Rietveld analysis points to an orthorhombic phase of the $CsPbBr_3$ NPs.[49] In our case, XRD has allowed the different compounds obtained after each synthesis (i.e., $CsPbBr_3$ and Cs_4PbBr_6) to be determined. The determination of the exact crystalline phase of each compound is beyond the scope of this work. It has been previously

Table 1. Experimental Details and Parameters of Synthesis with Different Temperatures[a]

temperature	130 °C	150 °C	170 °C
Pb:Sn (molar ratio)	1:2.5	1:2.5	1:2.5
time (s)	5	5	5
PL peak (nm)	499	503	503
FWHM	23.7	21.2	22.6
PLQY (%)	65.0 ± 0.7	73.4 ± 0.9	69.8 ± 1.3
Bandgap (eV)	2.45	2.43	2.39
Stokes shift	12 nm	10 nm	6 nm
	61.2 meV	50.0 meV	29.8 meV
XRD	*/#	*/#	*/#
Average Sn (%)	18.8 ± 1.0	7.0 ± 2.0	0
Average size (nm)	9 ± 6	6.2 ± 0.5	12 ± 3

[a]In all of the cases, the reaction time (5 s) and the precursor amount and ratio were fixed. The amount of $PbBr_2$ precursor in the synthesis was 0.166 mmol, and the amount of precursor $SnBr_2$ was 2.5 times higher. The amount of Cs-oleate was 0.045 mmol. Optical properties of the synthesized NPs have been measured on solution after synthesis and after washing allowing the following to be determined: the PL peak position, the full width at half-maximum (FWHM) of the PL peak, the PLQY, the bandgap extracted from the analysis of the Tauc plots of the absorption measurements, and finally the Stokes shift between light absorption and emission. XRD indicates the crystalline compounds detected by XRD, see Figure 1a, # = $CsXBr_3$ and * = Cs_4XBr_6, where X is Pb and Sn, the % of Sn measured by EDX during the TEM characterization is also indicated. The average size of the nanoparticles obtained by the statistical analysis of TEM images is also indicated; more detailed histograms with NP size can be found in Figure S6.

observed that both $CsPbBr_3$ and Cs_4PbBr_6 NPs[50] and even hybridized single nanoparticles of $CsPbBr_3/Cs_4PbBr_6$ can be obtained from the same synthesis.[51] The introduced Cs amount in our synthesis is higher than that in other procedures,[9] promoting the formation of Cs_4PbBr_6.[8] A detailed discussion of the results with other synthesis conditions can be found in section 1 of the Supporting Information, Figures S2−S5 and Tables S1 and S2.

The NPs have been optically characterized by absorption and emission spectroscopies; see Figure 1b. Just small variation on bandgap and PL peak can be observed depending on the temperature of reaction; see Figure 1b and Table 1. These NPs have small Stokes shifts (6−12 nm) between the absorption edge and the emission peak which are consistent with a direct exciton recombination process.[52−55] Previous literature presents different results about the optical properties of Cs_4PbBr_6, and the main controversial point is if this material has or does not have a strong PL emission.[39−41,50,56,57] In our case, samples just containing Cs_4PbBr_6 NPs present low PLQY, as we discuss below. Contrarily, samples containing $CsPbBr_3$ present high PLQY; see Table 1.

In order to characterize the morphology of the obtained NPs and the percentage of incorporated Sn, TEM characterization including EDX analysis of the NPs has been carried out. Typical cubical NPs corresponding to perovskite $CsPbBr_3$ have been observed for all of the growth conditions; see Figure 1c−e. Particles with hexagonal or rounded shape can also be observed corresponding to Cs_4PbBr_6 NPs and hybridized nanoparticles of $CsPbBr_3/Cs_4PbBr_6$,[50] respectively. The NPs synthesized at 150 °C are the ones that present a narrower size distribution (see Figure S6) and even can form superlattices using cubic perovskite NPs as building bricks (see Figure 1d).

DOI: 10.1021/acs.jpcc.8b02499
J. Phys. Chem. C XXXX, XXX, XXX−XXX

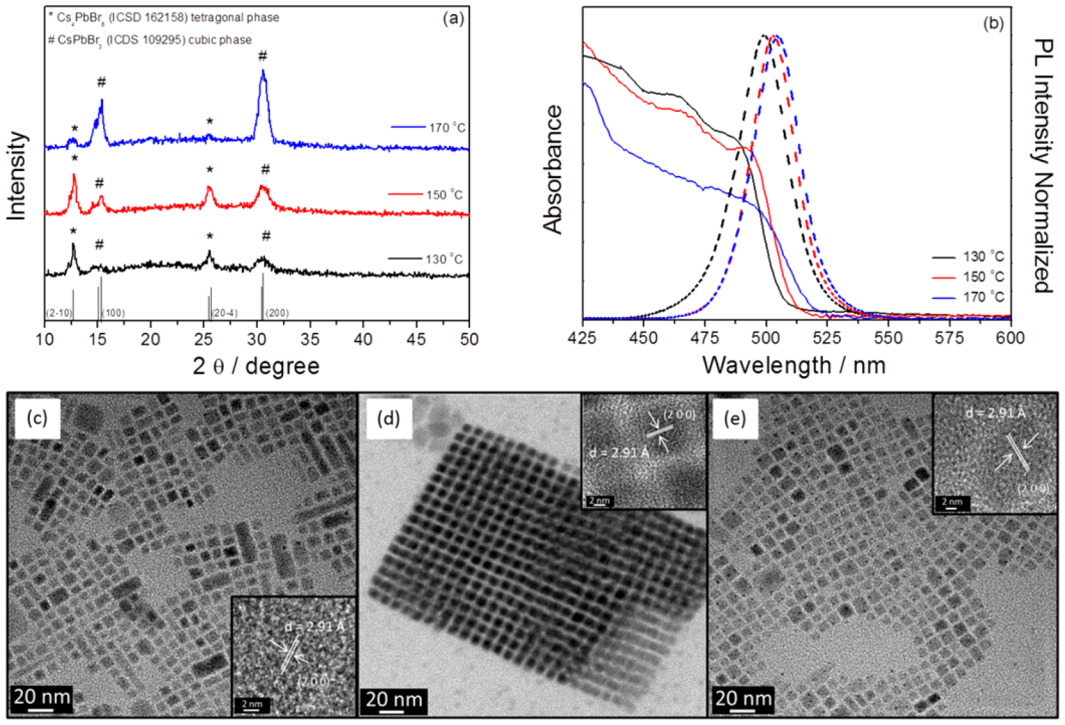

Figure 1. X-ray diffraction, optical absorption, and TEM images corresponding to different synthesis temperatures. (a) X-ray diffractograms, (b) absorption (solid lines) and emission spectra (dashed lines), and (c–e) TEM images of Cs–Pb–Sn–Br NPs with different synthesis temperatures: 130, 150, and 170 °C, respectively. The insets are the HRTEM images of $CsPbBr_3$ perovskite NPs as determined by the crystalline plane distance and EDX measurements.

Table 2. Experimental Details and Parameters of Synthesis with Different Precursor Concentrations[a]

molar ratio	Pb:Sn = 1:0	Pb:Sn = 1:1	Pb:Sn = 1:2.5	Pb:Sn = 3.5:0	Pb:Sn = 1:5
[Pb] (mmol)	0.166	0.166	0.166	0.581	0.166
[Sn] (mmol)	0	0.166	0.415	0	0.830
[Br] (mmol)	0.332	0.664	1.162	1.162	1.992
PL (nm)	513	509	503	507	488
FWHM	22.0	21.4	21.2	23.0	30.1
PLQY (%)	7.3 ± 1.2	62.8 ± 1.0	73.4 ± 0.9	45.7 ± 1.7	26.4 ± 3.3
Bandgap (eV)	∧	2.39	2.43	2.38	2.43
Stokes shift	∧	10 nm	10 nm	16 nm	14 nm
		50.0 meV	50.0 meV	79.7 meV	75.0 meV
XRD	*	#/*	#/*	*/#	*
Average Sn %	0	4.0 ± 1.0	7.0 ± 2.0	0	12.0 ± 3.0
Average size (nm)	17.89 ± 2.73	10.81 ± 1.27	6.18 ± 0.48	9.18 ± 1.14	84.97 ± 6.58

[a]Reaction temperature and reaction time were fixed to 150 °C and 5 s, respectively. The amount of Pb, Sn, and Br, introduced by $PbBr_2$ and $SnBr_2$ precursors, is indicated, while the amount of Cs-oleate precursor is fixed to 0.045 mmol. Two conditions for pure-Pb NP have been investigated, one with 0.166 mmol of $PbBr_2$ (ratio 1:0) and the other with a 3.5 times higher amount (ratio 3.5:0). Optical properties of the synthesized NPs have been measured on solution after synthesis and after washing allowing the following to be determined: the PL peak position, the full width at half-maximum (FWHM) of the PL peak, the PLQY, the bandgap extracted from the analysis of the Tauc plots of the absorption measurements, and finally the Stokes shift between light absorption and emission. The bandgap and Stokes shift are not indicated for samples with ratio 1:0, as no clear band edge was observed. XRD indicates the crystalline compounds detected by XRD, see Figure 1a, # = $CsPbBr_3$ cubic phase (ICDS 109295) and * = Cs_4PbBr_6 tetragonal phase (ICDS 162158), where X is Pb and Sn, the % of Sn measured by EDX during the TEM characterization is also indicated. The average size of the nanoparticles obtained by the statistical analysis of TEM images is also indicated; more detailed histograms with NP size can be found in Figure S9. ∧ = For the Pb:Sn 1:0 sample, the absorption band edge was not easy to determine from the experimental results and consequently the bandgap and the Stokes shift cannot be calculated without a big error.

EDX analysis of NPs has allowed determining the percentage of Sn incorporation. The incorporation of Sn is higher as the reaction temperature decreases with a maximum value of incorporation close to 19% for T = 130 °C, as can be seen with more details in Figure S7. However, the most interesting result is that this relative high incorporation of Sn does not imply a significant reduction of PLQY, 65%, with respect to NP samples where Sn is not incorporated, as the ones grown at 170 °C, with a PLQY of 69.8%; see Table 1. In fact, the highest PLQY, 74.3%, has been obtained for the samples grown at 150 °C where 7% of Sn was incorporated. High resolution TEM (HRTEM) points to an incorporation of Sn into $CsPbBr_3$ NPs; see Table S3. Variations of the synthesis method reported in

DOI: 10.1021/acs.jpcc.8b02499
J. Phys. Chem. C XXXX, XXX, XXX−XXX

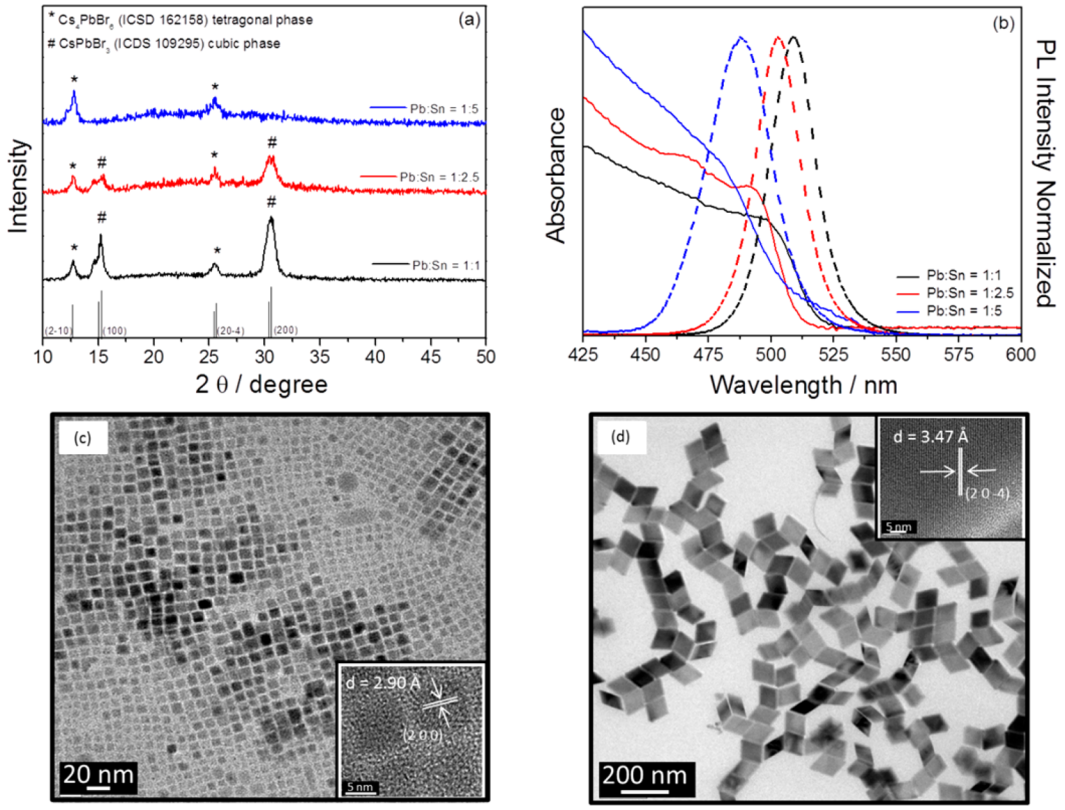

Figure 2. Comparison among different molar ratio (Pb:Sn) synthesis. (a) Absorption and emission spectra, (b) X-ray diffractograms, and (c and d) TEM images of Cs−Pb−Sn−Br NPs with different molar ratio synthesis (Pb:Sn) of 1:1 and 1:5, respectively. The insets are the HRTEM images. NPs synthesized with molar ratio synthesis (Pb:Sn) 1:2.5 can be observed in Figure 1d. Comparative TEM images of the complete series as a function of precursor ratio can be found in Figure S8.

section 3 have also been analyzed (see section 1 in the Supporting Information), but lower PLQY was obtained.

The EDX measurements were performed on areas containing a large number of nanocrystals, in order to obtain a statistically relevant result. The percentage of Sn incorporated depends on the nature of the NP; see Figure S7. Higher incorporation is observed for $CsPbBr_3$ rather than for Cs_4PbBr_6. This fact is under current research. The incorporation of Sn produces a blue shift of light absorption spectra and PL emission, in good agreement with previous results of Sn incorporation.[31,32] Note that the quantum confinement for sizes lower than the Bohr diameter (12−14 nm)[9,58,59] also produces a blue shift. Samples grown at 130 and 150 °C present a NP average size of 9 nm and 6.2 nm, respectively, but the former exhibit a larger emission blue shift due to the higher Sn incorporation.

4.2. Pb and Sn Precursor Ratio. As a second step in the systematic characterization of the Sn incorporation as a function of the synthesis conditions, the effect of Sn precursor concentration on the nature and properties of the NPs has been analyzed. The reaction time at 5 s and the reaction temperature at 150 °C have been fixed. This temperature was chosen, as it allows the incorporation of Sn and an excellent PLQY; see Table 1. The amount of $PbBr_2$ precursor was fixed to 0.166 mmol, and $SnBr_2$ precursor was added in different ratios of 1:0 (pure-Pb perovskite), 1:1, 1:2.5, and 1:5. Owing to the analysis of the effect of Br amount in the synthesis without the incorporation of Sn, two different synthesis procedures have been analyzed, one using the standard conditions of $PbBr_2$, 0.166 mmol, and another incrementing the $PbBr_2$ amount by 3.5 times, denoted as a Pb:Sn ratio of 1:0 and 3.5:0, respectively.

EDX indicates an enhancement of Sn incorporation with the increase of Sn precursor ratio, as should be expected. The maximum Sn incorporated into the NPs on average is 12% for Pb:Sn 1:5 precursor ratio; see Table 2. The nature of the NP synthesized is strongly dependent on the precursor ratio. XRD indicates the presence of both compounds $CsPbBr_3$ and Cs_4PbBr_6 for precursor ratios of 1:1 and 1:2.5, while for ratios 1:0 and 1:5 just the Cs_4PbBr_6 was obtained; see Figure 2a. The incorporation of Sn produces a blue shift in the absorption and emission spectra, as shown in Figure 2b, in good agreement with previous results of Sn incorporation.[31,32] A low PLQY was observed for samples without perovskite $CsPbBr_3$ NPs, for samples with precursor ratios 1:0 and 1:5, indicating that the high PLQY observed for the 1:1 and 1:2.5 molar ratios arises from the presence of perovskite NPs; see Table 2. The highest PLQY has been obtained for a precursor ratio of 1:2.5. The sample with precursor ratio 1:1 maintains a PLQY higher than 60%, and $CsPbBr_3$ NPs were detected by XRD and TEM micrographs; see Figure 2c. However, the sample with a 1:5 ratio was formed by relatively bigger Cs_4PbBr_6 NPs; see Figure 2d. In this sample, 12% of Sn was incorporated. For NPs synthesized with a 1:5 precursor ratio, the long-term stability is also poor, colloidal solution precipitates and so the PLQY is lost after a few days, while the NP solutions are stable for months with no decrease of PLQY for the other ratios.

Only Cs_4PbBr_6 NPs were observed when no Sn precursor was added (1:0 ratio) and just $PbBr_2$ precursor was used. The addition of $SnBr_2$ (1:1 and 1:2.5 ratios), maintaining the

DOI: 10.1021/acs.jpcc.8b02499
J. Phys. Chem. C XXXX, XXX, XXX−XXX

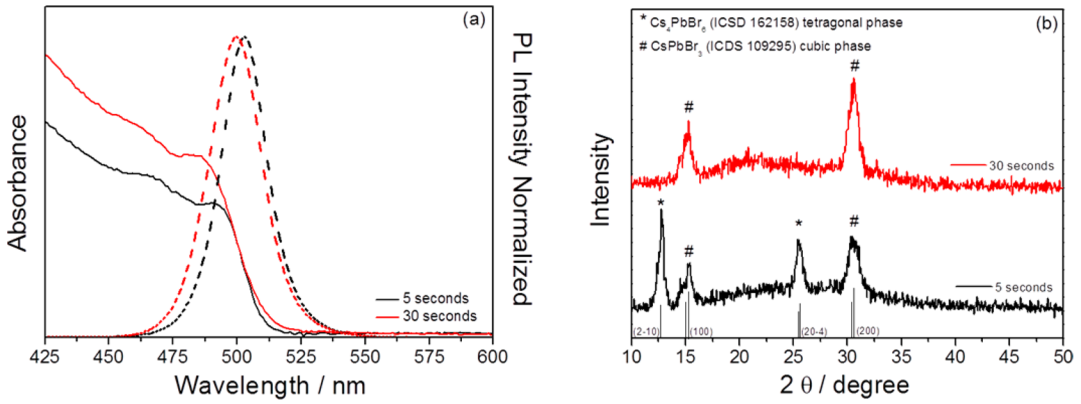

Figure 3. Comparison between different reaction times: (a) absorption and emission spectra; (b) X-ray diffractograms. Comparative TEM images of the complete series as a function of precursor ratio can be found in Figure S11.

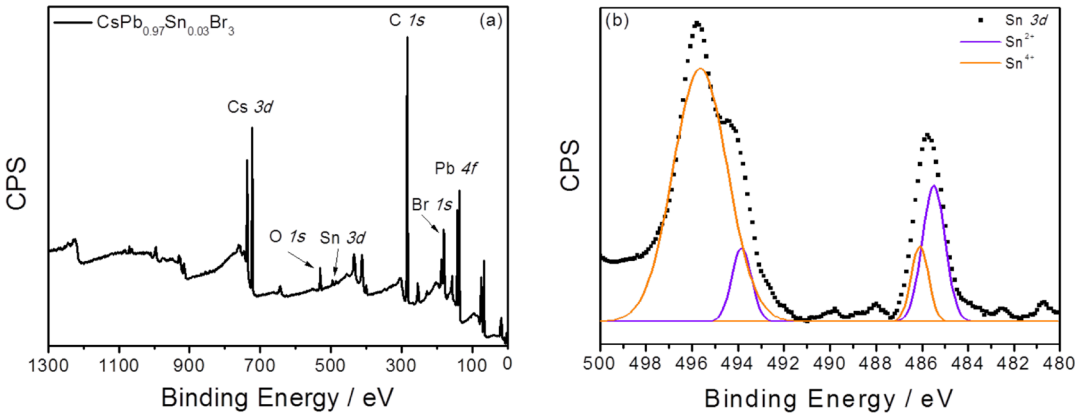

Figure 4. (a) XPS exploratory spectra and (b) high resolution XPS spectra of Sn. High resolution spectra for Cs, Pb, and Br can be found in Figure S9.

amount of $PbBr_2$, releases a part of $PbBr_2$ that can react with Cs_4PbBr_6 to form $CsPbBr_3$, following the chemical reaction $Cs_4PbBr_6 + 3PbBr_2 \rightarrow 4CsPbBr_3$.[50] However, this trend was broken for 1:5 where again just Cs_4PbBr_6 NPs are obtained, as we can see by comparing parts a and d of Figure 2. Despite that both 1:0 and 1:5 ratios produce Cs_4PbBr_6 NPs, the shape is very different (compare parts c and d of Figure 2), indicating that Sn plays an important role in the NP morphology, obtaining small truncated trapezoidal Cs_4PbBr_6 nanoparticles when just Br precursor was used in the synthesis (1:0 ratio) and large rhombohedra NPs for a precursor ratio of 1:5.

The increase of Sn ratio with respect to Pb is obtained by the addition of $SnBr_2$ precursor. This addition not only affects the metallic cation but also the amount of Br anion. While an excess of Pb in NPs would act as trap states, resulting in a PL quenching,[60] the excess halogen ions have been used to enrich the perovskite NP surfaces, resulting in a self-passivation effect of Pb ions. Halogen-rich perovskite NPs inhibit the electrons trapped on surface defects, culminating in a high PLQY when NPs are synthesized with an excess of halide precursor.[61−63] To evaluate to what extent the Br-rich synthesis conditions ($PbBr_2$ + $SnBr_2$) or the partial substitution of Pb by Sn influence the obtained high PLQY, two different syntheses of pure-Pb NPs were prepared, named 1:0 and 3.5:0; see Table 2. A comparative analysis of the XRD, absorption, and emission spectra can be found in Figure S10. The increase of PLQY under Br-rich conditions (from 7.3% for ratio 1:0 to 45.7% for ratio 3.5:0) can be justified by the presence of $CsPbBr_3$ NPs, observed under 3.5:0 growth conditions (see Figure S10) and not at 1:0, and also by the self-passivation of rich halide synthesis conditions.[61−63]

4.3. Reaction Time. The last part of our study focused on the reaction time. Two different reaction times, 5 and 30 s, were analyzed, while all of the other synthesis parameters were maintained fixed, i.e., T = 150 °C and Pb:Sn precursor ratio 1:2.5; see Table S4. Similar optical features have been obtained in both cases; see Figure 3a. For 30 s of reaction time, just $CsPbBr_3$ NPs were obtained; see Figure 3b. Longer reaction times produce an increase of NP size from 6 to 10 nm on average; see Table S4. In addition, no replacement of Pb by Sn was detected for 30 s reaction time, suggesting that Sn is incorporated during the onset NP formation, as also suggested when Mn^{2+} was incorporated into $CsPbBr_3$ NP.[33] We have also observed that the Sn incorporated is replaced by Pb for the longer reaction time. For a 5 s reaction time, 7% of Pb was replaced by Sn, and for 30 s reaction time, no Sn was incorporated into the NPs; see Table S4. The Sn-replacing is a process of external impurity additions,[64] in which for longer synthesis time the crystal will tend to self-purify.

Interestingly, despite that just $CsPbBr_3$ are obtained in the synthesis with longer reaction time, the PLQY reduces from 73.4 to 64.7% and the size distribution is larger (see Figure S12), in good agreement with previous works.[58] On the other hand, the fwhm is lower for 5 s reaction time (see Table S4), in good agreement with the results of Koolyk et al.[58]

DOI: 10.1021/acs.jpcc.8b02499
J. Phys. Chem. C XXXX, XXX, XXX−XXX

5. DISCUSSION

The results shown in the previous section indicate that Pb has been partially substituted by Sn in the synthesized NPs. However, the most interesting result is that this incorporation has been made with no cost, or even an enhancement, of the PLQY in contrast with previous works where a deleterious effect on the optical properties was observed after Sn incorporation.[30−32] An increase of performance was only obtained for a small substitution of 0.3% of Pb by Sn.[44] In contrast, here we report PLQYs as high as 65.0 and 73.4% for NPs where 18.8 and 7% of Pb was replaced by Sn, respectively; see Table 1. As far as we know, this is the first report of less-Pb halide perovskites, containing a substantial amount of Sn, in which the optical properties improve with respect to the pure-Pb perovskite. Previous results pointed to a PLQY reduction when Sn was replacing Pb in a substantial amount, which was mainly attributed to the unstable Sn oxidation under ambient conditions.[32,43] The reported PLQY decrease implies a trap state contribution, which could result in an undesirable conversion of Sn^{2+} to Sn^{4+}, being that Sn^{4+} is a more stable state than Sn^{2+} under ambient conditions.[30]

XPS has been used to determine the electronic state of the elements present in the synthesized NPs; see Figure 4a. The sample with the highest PLQY has been analyzed, T = 150 °C, Pb:Sn = 1:2.5 molar ratio, and reaction time 5 s; see Table 1. XPS spectra can be visualized in Figure 4a. The XPS spectrograph showed two characteristic peaks corresponding to Sn ($3d_{5/2}$, $3d_{3/2}$) with positions of 485.7 and 495.8 eV, respectively, as shown in Figure 4b. The binding energy of the Sn $3d_{5/2}$ peak is likely assigned to Sn^{2+} following the previous bibliography.[65,66] However, the Sn $3d_{3/2}$ peak showed a deformation which is related with a coexistence of oxidation states Sn^{4+} and Sn^{2+}. Despite that a partial oxidation of Sn^{2+} took place, it is important to emphasize that XPS measurements were performed 3 months after NP synthesis and were measured in the USA while samples were grown in Spain, pointing to a significant long-term stabilization of Sn^{2+} cations. In fact, the PLQY of record NP solution has been measured along several months, with no change in value, pointing in the same direction of long-term stable samples. Sn^{2+} are prone to oxidation, and stabilization requires blocking this process.[34] The most likely reason for this Sn^{2+} cation significant stabilization would be the higher ligand content on the NP synthesis protecting the NP core from external oxidation. Comparison with other synthesis recipes with a lower amount of ligand concentration during the synthesis is discussed in Supporting Information section 1. The XPS spectrograph of the other elements Cs, Pb, and Br is reported in Figure S13. Peak positions of the different elements detected by XPS are shown in Table S5.

Moreover, samples prepared with the same amount of halide as ratio 1:2.5 and 3.5:0 show that the former where 7% Pb is replaced by Sn presents a higher PLQY; see Table 2. Thus, the highest PLQY observed could not be attributed just to Br-rich conditions but also to Sn-replacing, which further improves the optical properties of perovskite NPs with larger PLQY, smaller Stokes shift. and narrower fwhm; see Table 2. Unveiling the exact reason why the incorporation of stabilized Sn^{2+} replacing Pb^{2+} produces an improvement of optical properties will require further research. Wang et al. observed an increase of performance with the addition of Sn that was attributed to the suppression of trion generation by Sn doping.[44] However, in their case, the amount of Sn incorporated was sensibly lower, 0.3%, and Sn was oxidized as Sn^{4+}. Very recently, it has been suggested that the reduction in the bond length between metallic cation and halide in $CsPbX_3$ (X = Cl, Br, I) perovskites by partial substitution of Pb^{2+} cation can increase the stability of the all-inorganic $CsPbX_3$ perovskite, thereby improving the stability of their solar cells, emission spectra, and other properties.[67] The results reported here point in this direction of an increase of performance with incorporation of Sn, if Sn can preserve to a significant extent its Sn^{2+} oxidation state, as has been observed in the results reported here. Theoretical calculation will help to clarify this point as well as the role of ligands in Sn^{2+} stabilization.

6. CONCLUSIONS

In summary, we have carried out a detailed study of Cs−Pb−Sn−Br NP formation depending on different synthesis parameters such as reaction time, temperature, and Pb:Sn precursor ratio. Different properties of the synthesized particles have been studied, as the kind of NPs formed, the PLQY, and the Sn content, which were analyzed by EDX in the TEM measurements. We observed the formation of cubic perovskite $CsPbBr_3$ and tetragonal Cs_4PbBr_6 depending on the growth conditions. The presence of the cubic phase increases with growth temperature and reaction time. The incorporation of Sn increases at low reaction temperature and for small reaction time, and also with high Sn precursor concentration. The highest Sn incorporation observed in the experiments here reported is close to 19% on average. In contrast with previous reports where the partial incorporation of Sn in the place of Pb in a substantial amount always produced a decrease of the optical properties, i.e., the PLQY and FWHM, here an enhancement is observe. At this point, we have shown the improvement of these optical properties with Sn incorporation. PLQYs as high as 73.4% have been obtained with 7% of Pb replaced by Sn, higher than the one obtained for pure-Pb NPs. We have ruled out the possibility that this enhancement is originated just by the synthesis with Br-rich conditions. Improvement of Br amount during NP synthesis produces a self-passivation by the halide excess contributing to the enhancement of the optical properties but cannot justify completely the strong improvement of these properties observed when Sn is also incorporated. Undoubtedly, the significant stabilization of Sn^{2+} in the NPs even several months after NP preparation, as has been determined by XPS measurements, is a key point to explain this outstanding behavior. The presence of large surface ligand concentration is likely helping in the stabilization of Sn^{2+} protecting it from oxidation. The reduction in the bond length between metallic cation and halide by the incorporation of Sn producing an increase of stability and an enhancement of optical properties[67] is a feasible hypothesis to explain the obtained results; however, further research will be needed to confirm it. Further research will help to identify the exact mechanism of stabilization and the incremental role of Sn-replacing. The result here reported could have an important implication to obtain less-Pb and Pb-free perovskite materials with excellent properties and stability.

■ ASSOCIATED CONTENT

Supporting Information

The Supporting Information is available free of charge on the ACS Publications website at DOI: 10.1021/acs.jpcc.8b02499.

DOI: 10.1021/acs.jpcc.8b02499
J. Phys. Chem. C XXXX, XXX, XXX−XXX

Figure with crystalline structure of cubic phase and tetragonal phase of perovskites, analysis of the results with other synthesis conditions than the ones reported in the main text, which includes table with experimental details and parameters of different synthesis methods with and without Sn-replacing, comparatives figures among the two different synthesis methods which contain X-ray diffractograms, absorption and PL emission spectra, TEM images, size distribution histograms, and XPS results of samples synthesized at 130 °C, with different Br concentration synthesis, and different synthesis times (5 and 30 s) (PDF)

AUTHOR INFORMATION

Corresponding Author

*E-mail: sero@uji.es.

ORCID

Marco Antônio Schiavon: 0000-0002-1553-5388

Iván Mora-Seró: 0000-0003-2508-0994

Notes

The authors declare no competing financial interest.

ACKNOWLEDGMENTS

We acknowledge the outstanding work of Prof. Prashant Kamat in Physical Chemistry especially in the field of quantum dots inspiring a large number of researchers, including us. This work was partially supported by European Research Council (ERC) via Consolidator Grant (724424 - No-LIMIT). FAPEMIG, Rede Mineira de Química (RQ-MG), CNPq and CAPES, the Spanish Ministry of Economy and Competitiveness (MINECO) under the project TEC2014-60173 and the Generalitat Valenciana under the project Prometeo II 2015/004. The present work was developed with support from CAPES (Coordination of Improvement of Higher Level Personnel). We acknowledge SCIC from UJI for help with XRD characterization, the SCSIE-University of Valencia for providing TEM facilities, and Molecular Foundry of Lawrence Berkeley National Laboratory USA by XPS measurements and CONACyT-SENER -2015-07 Project 269386.

REFERENCES

(1) Stranks, S. D.; Snaith, H. J. Metal-halide perovskites for photovoltaic and light-emitting devices. *Nat. Nanotechnol.* **2015**, *10*, 391−402.

(2) Yang, W. S.; Park, B.-W.; Jung, E. H.; Jeon, N. J.; Kim, Y. C.; Lee, D. U.; Shin, S. S.; Seo, J.; Kim, E. K.; Noh, J. H.; et al. Iodide management in formamidinium-lead-halide−based perovskite layers for efficient solar cells. *Science* **2017**, *356*, 1376−1379.

(3) Xiao, Z.; Kerner, R. A.; Zhao, L.; Tran, N. L.; Lee, K. M.; Koh, T.-W.; Scholes, G. D.; Rand, B. P. Efficient perovskite light-emitting diodes featuring nanometre-sized crystallites. *Nat. Photonics* **2017**, *11*, 108−115.

(4) Jing, L.; Kershaw, S. V.; Li, Y.; Huang, X.; Rogach, A. L.; Gao, M. Aqueous Based Semiconductor Nanocrystals. *Chem. Rev.* **2016**, *116*, 10623−10730.

(5) Byrne, S. J.; le Bon, B.; Corr, S. A.; Stefanko, M.; O'Connor, C.; Gun'ko, Y. K.; Rakovich, Y. P.; Donegan, J. F.; Williams, Y.; Volkov, Y.; et al. Synthesis, characterisation, and biological studies of CdTe quantum dot-naproxen conjugates. *ChemMedChem* **2007**, *2*, 183−186.

(6) Shen, H.; Cao, W.; Shewmon, N. T.; Yang, C.; Li, L. S.; Xue, J. High-efficiency, low turn-on voltage blue-violet quantum-dot-based light-emitting diodes. *Nano Lett.* **2015**, *15*, 1211−1216.

(7) Zhang, Y.; Xie, C.; Su, H.; Liu, J.; Pickering, S.; Wang, Y.; Yu, W. W.; Wang, J.; Hahm, J. I.; Dellas, N.; et al. Employing heavy metal-free colloidal quantum dots in solution-processed white light-emitting diodes. *Nano Lett.* **2011**, *11*, 329−332.

(8) Schmidt, L. C.; Pertegas, A.; Gonzalez-Carrero, S.; Malinkiewicz, O.; Agouram, S.; Minguez Espallargas, G.; Bolink, H. J.; Galian, R. E.; Perez-Prieto, J. Nontemplate synthesis of $CH_3NH_3PbBr_3$ perovskite nanoparticles. *J. Am. Chem. Soc.* **2014**, *136*, 850−853.

(9) Protesescu, L.; Yakunin, S.; Bodnarchuk, M. I.; Krieg, F.; Caputo, R.; Hendon, C. H.; Yang, R. X.; Walsh, A.; Kovalenko, M. V. Nanocrystals of Cesium Lead Halide Perovskites (CsPbX(3), X = Cl, Br, and I): Novel Optoelectronic Materials Showing Bright Emission with Wide Color Gamut. *Nano Lett.* **2015**, *15*, 3692−3696.

(10) Nair, V. C.; Muthu, C.; Rogach, A. L.; Kohara, R.; Biju, V. Channeling Exciton Migration into Electron Transfer in Formamidinium Lead Bromide Perovskite Nanocrystal/Fullerene Composites. *Angew. Chem., Int. Ed.* **2017**, *56*, 1214−1218.

(11) Davis, N. J.; de la Pena, F. J.; Tabachnyk, M.; Richter, J. M.; Lamboll, R. D.; Booker, E. P.; Wisnivesky Rocca Rivarola, F.; Griffiths, J. T.; Ducati, C.; Menke, S. M.; Deschler, F.; Greenham, N. C.; et al. Photon Reabsorption in Mixed CsPbCl3:CsPbI3 Perovskite Nanocrystal Films for Light-Emitting Diodes. *J. Phys. Chem. C* **2017**, *121*, 3790−3796.

(12) Isarov, M.; Tan, L. Z.; Bodnarchuk, M. I.; Kovalenko, M. V.; Rappe, A. M.; Lifshitz, E. Rashba Effect in a Single Colloidal $CsPbBr_3$ Perovskite Nanocrystal Detected by Magneto-Optical Measurements. *Nano Lett.* **2017**, *17*, 5020−5026.

(13) Bhooshan Kumar, V.; Gouda, L.; Porat, Z.; Gedanken, A. Sonochemical synthesis of $CH_3NH_3PbI_3$ perovskite ultrafine nanocrystal sensitizers for solar energy applications. *Ultrason. Sonochem.* **2016**, *32*, 54−59.

(14) Perumal, A.; Shendre, S.; Li, M.; Tay, Y. K.; Sharma, V. K.; Chen, S.; Wei, Z.; Liu, Q.; Gao, Y.; Buenconsejo, P. J.; et al. High brightness formamidinium lead bromide perovskite nanocrystal light emitting devices. *Sci. Rep.* **2016**, *6*, 36733.

(15) Gonzalez-Carrero, S.; Galian, R. E.; Perez-Prieto, J. Organic-inorganic and all-inorganic lead halide nanoparticles. *Opt. Express* **2016**, *24*, A285−301.

(16) Veldhuis, S. A.; Boix, P. P.; Yantara, N.; Li, M.; Sum, T. C.; Mathews, N.; Mhaisalkar, S. G. Perovskite Materials for Light-Emitting Diodes and Lasers. *Adv. Mater.* **2016**, *28*, 6804−6834.

(17) Song, J.; Li, J.; Li, X.; Xu, L.; Dong, Y.; Zeng, H. Quantum Dot Light-Emitting Diodes Based on Inorganic Perovskite Cesium Lead Halides ($CsPbX_3$). *Adv. Mater.* **2015**, *27*, 7162−7167.

(18) Zhang, X.; Lin, H.; Huang, H.; Reckmeier, C.; Zhang, Y.; Choy, W. C.; Rogach, A. L. Enhancing the Brightness of Cesium Lead Halide Perovskite Nanocrystal Based Green Light-Emitting Devices through the Interface Engineering with Perfluorinated Ionomer. *Nano Lett.* **2016**, *16*, 1415−1420.

(19) Swarnkar, A.; Marshall, A. R.; Sanehira, E. M.; Chernomordik, B. D.; Moore, D. T.; Christians, J. A.; Chakrabarti, T.; Luther, J. M. Quantum dot-induced phase stabilization of alpha-$CsPbI_3$ perovskite for high-efficiency photovoltaics. *Science* **2016**, *354*, 92−95.

(20) Kojima, A.; Teshima, K.; Shirai, Y.; Miyasaka, T. Organometal halide perovskites as visible-light sensitizers for photovoltaic cells. *J. Am. Chem. Soc.* **2009**, *131*, 6050−6051.

(21) Saidaminov, M. I.; Haque, M. A.; Savoie, M.; Abdelhady, A. L.; Cho, N.; Dursun, I.; Buttner, U.; Alarousu, E.; Wu, T.; Bakr, O. M. Perovskite Photodetectors Operating in Both Narrowband and Broadband Regimes. *Adv. Mater.* **2016**, *28*, 8144−8149.

(22) Dong, Y.; Gu, Y.; Zou, Y.; Song, J.; Xu, L.; Li, J.; Xue, J.; Li, X.; Zeng, H. Improving All-Inorganic Perovskite Photodetectors by Preferred Orientation and Plasmonic Effect. *Small* **2016**, *12*, 5622−5632.

(23) Swarnkar, A.; Marshall, A. R.; Sanehira, E. M.; Chernomordik, B. D.; Moore, D. T.; Christians, J. A.; Chakrabarti, T.; Luther, J. M. Quantum dot−induced phase stabilization of α-$CsPbI_3$ perovskite for high-efficiency photovoltaics. *Science* **2016**, *354*, 92−95.

(24) Sanehira, E. M.; Marshall, A. R.; Christians, J. A.; Harvey, S. P.; Ciesielski, P. N.; Wheeler, L. M.; Schulz, P.; Lin, L. Y.; Beard, M. C.; Luther, J. M. Enhanced mobility $CsPbI_3$ quantum dot arrays for

DOI: 10.1021/acs.jpcc.8b02499
J. Phys. Chem. C XXXX, XXX, XXX−XXX

record-efficiency, high-voltage photovoltaic cells. *Science Advances* **2017**, *3*, eaao4204.
(25) Jellicoe, T. C.; Richter, J. M.; Glass, H. F.; Tabachnyk, M.; Brady, R.; Dutton, S. E.; Rao, A.; Friend, R. H.; Credgington, D.; Greenham, N. C.; et al. Synthesis and Optical Properties of Lead-Free Cesium Tin Halide Perovskite Nanocrystals. *J. Am. Chem. Soc.* **2016**, *138*, 2941−2944.
(26) Hao, F.; Stoumpos, C. C.; Cao, D. H.; Chang, R. P. H.; Kanatzidis, M. G. Lead-free solid-state organic-inorganic halide perovskite solar cells. *Nat. Photonics* **2014**, *8*, 489−494.
(27) Kumar, M. H.; Dharani, S.; Leong, W. L.; Boix, P. P.; Prabhakar, R. R.; Baikie, T.; Shi, C.; Ding, H.; Ramesh, R.; Asta, M.; et al. Lead-free halide perovskite solar cells with high photocurrents realized through vacancy modulation. *Adv. Mater.* **2014**, *26*, 7122−7127.
(28) Takahashi, Y.; Obara, R.; Lin, Z.-Z.; Takahashi, Y.; Naito, T.; Inabe, T.; Ishibashi, S.; Terakura, K. Charge-transport in tin-iodide perovskite $CH_3NH_3SnI_3$: origin of high conductivity. *Dalton Transactions* **2011**, *40*, 5563−5568.
(29) Takahashi, Y.; Hasegawa, H.; Takahashi, Y.; Inabe, T. Hall mobility in tin iodide perovskite $CH_3NH_3SnI_3$: Evidence for a doped semiconductor. *J. Solid State Chem.* **2013**, *205*, 39−43.
(30) Swarnkar, A.; Ravi, V. K.; Nag, A. Beyond Colloidal Cesium Lead Halide Perovskite Nanocrystals: Analogous Metal Halides and Doping. *ACS Energy Letters* **2017**, *2*, 1089−1098.
(31) van der Stam, W.; Geuchies, J. J.; Altantzis, T.; van den Bos, K. H.; Meeldijk, J. D.; Van Aert, S.; Bals, S.; Vanmaekelbergh, D.; de Mello Donega, C. Highly Emissive Divalent-Ion-Doped Colloidal $CsPb_{1-x}Mn_xBr_3$ Perovskite Nanocrystals through Cation Exchange. *J. Am. Chem. Soc.* **2017**, *139*, 4087−4097.
(32) Zhang, X.; Cao, W.; Wang, W.; Xu, B.; Liu, S.; Dai, H.; Chen, S.; Wang, K.; Sun, X. W. Efficient light-emitting diodes based on green perovskite nanocrystals with mixed-metal cations. *Nano Energy* **2016**, *30*, 511−516.
(33) Guria, A. K.; Dutta, S. K.; Adhikari, S. D.; Pradhan, N. Doping Mn^{2+} in Lead Halide Perovskite Nanocrystals: Successes and Challenges. *ACS Energy Letters* **2017**, *2*, 1014−1021.
(34) Leijtens, T.; Prasanna, R.; Gold-Parker, A.; Toney, M. F.; McGehee, M. D. Mechanism of Tin Oxidation and Stabilization by Lead Substitution in Tin Halide Perovskites. *ACS Energy Letters* **2017**, *2*, 2159−2165.
(35) Zhao, D.; Yu, Y.; Wang, C.; Liao, W.; Shrestha, N.; Grice, C. R.; Cimaroli, A. J.; Guan, L.; Ellingson, R. J.; Zhu, K.; et al. Low-bandgap mixed tin−lead iodide perovskite absorbers with long carrier lifetimes for all-perovskite tandem solar cells. *Nature Energy* **2017**, *2*, 17018.
(36) Akkerman, Q. A.; Motti, S. G.; Srimath Kandada, A. R.; Mosconi, E.; D'Innocenzo, V.; Bertoni, G.; Marras, S.; Kamino, B. A.; Miranda, L.; De Angelis, F.; et al. Solution Synthesis Approach to Colloidal Cesium Lead Halide Perovskite Nanoplatelets with Monolayer-Level Thickness Control. *J. Am. Chem. Soc.* **2016**, *138*, 1010−1016.
(37) Zhang, D.; Eaton, S. W.; Yu, Y.; Dou, L.; Yang, P. Solution-Phase Synthesis of Cesium Lead Halide Perovskite Nanowires. *J. Am. Chem. Soc.* **2015**, *137*, 9230−9233.
(38) Bekenstein, Y.; Koscher, B. A.; Eaton, S. W.; Yang, P.; Alivisatos, A. P. Highly Luminescent Colloidal Nanoplates of Perovskite Cesium Lead Halide and Their Oriented Assemblies. *J. Am. Chem. Soc.* **2015**, *137*, 16008−16011.
(39) Yin, J.; Zhang, Y.; Bruno, A.; Soci, C.; Bakr, O. M.; Brédas, J.-L.; Mohammed, O. F. Intrinsic Lead Ion Emissions in Zero-Dimensional Cs_4PbBr_6 Nanocrystals. *ACS Energy Letters* **2017**, *2*, 2805−2811.
(40) Liu, Z.; Bekenstein, Y.; Ye, X.; Nguyen, S. C.; Swabeck, J.; Zhang, D.; Lee, S. T.; Yang, P.; Ma, W.; Alivisatos, A. P. Ligand Mediated Transformation of Cesium Lead Bromide Perovskite Nanocrystals to Lead Depleted Cs_4PbBr_6 Nanocrystals. *J. Am. Chem. Soc.* **2017**, *139*, 5309−5312.
(41) Akkerman, Q. A.; Park, S.; Radicchi, E.; Nunzi, F.; Mosconi, E.; De Angelis, F.; Brescia, R.; Rastogi, P.; Prato, M.; Manna, L. Nearly Monodisperse Insulator Cs_4PbX_6 (X = Cl, Br, I) Nanocrystals, Their Mixed Halide Compositions, and Their Transformation into $CsPbX_3$ Nanocrystals. *Nano Lett.* **2017**, *17*, 1924−1930.
(42) Li, G.; Wang, H.; Zhu, Z.; Chang, Y.; Zhang, T.; Song, Z.; Jiang, Y. Shape and phase evolution from $CsPbBr_3$ perovskite nanocubes to tetragonal $CsPb_2Br_5$ nanosheets with an indirect bandgap. *Chem. Commun.* **2016**, *52*, 11296−11299.
(43) Liu, F.; Ding, C.; Zhang, Y.; Ripolles, T. S.; Kamisaka, T.; Toyoda, T.; Hayase, S.; Minemoto, T.; Yoshino, K.; Dai, S.; et al. Colloidal Synthesis of Air-Stable Alloyed CsSn1−xPbxI3 Perovskite Nanocrystals for Use in Solar Cells. *J. Am. Chem. Soc.* **2017**, *139*, 16708−16719.
(44) Wang, H.-C.; Wang, W.; Tang, A.-C.; Tsai, H.-Y.; Bao, Z.; Ihara, T.; Yarita, N.; Tahara, H.; Kanemitsu, Y.; Chen, S.; et al. High-Performance $CsPb_{1-x}Sn_xBr_3$ Perovskite Quantum Dots for Light-Emitting Diodes. *Angew. Chem.* **2017**, *129*, 13838−13842.
(45) Liu, H.; Wu, Z.; Shao, J.; Yao, D.; Gao, H.; Liu, Y.; Yu, W.; Zhang, H.; Yang, B. $CsPb_xMn_{1-x}Cl_3$ Perovskite Quantum Dots with High Mn Substitution Ratio. *ACS Nano* **2017**, *11*, 2239−2247.
(46) Huang, H.; Polavarapu, L.; Sichert, J. A.; Susha, A. S.; Urban, A. S.; Rogach, A. L. Colloidal lead halide perovskite nanocrystals: synthesis, optical properties and applications. *NPG Asia Mater.* **2016**, *8*, e328.
(47) Bai, S.; Yuan, Z.; Gao, F. Colloidal metal halide perovskite nanocrystals: synthesis, characterization, and applications. *J. Mater. Chem. C* **2016**, *4*, 3898−3904.
(48) Protesescu, L.; Yakunin, S.; Bodnarchuk, M. I.; Krieg, F.; Caputo, R.; Hendon, C. H.; Yang, R. X.; Walsh, A.; Kovalenko, M. V. Nanocrystals of Cesium Lead Halide Perovskites (CsPbX3, X = Cl, Br, and I): Novel Optoelectronic Materials Showing Bright Emission with Wide Color Gamut. *Nano Lett.* **2015**, *15*, 3692−3696.
(49) Cottingham, P.; Brutchey, R. L. On the crystal structure of colloidally prepared CsPbBr3 quantum dots. *Chem. Commun.* **2016**, *52*, 5246−5249.
(50) Palazon, F.; Urso, C.; De Trizio, L.; Akkerman, Q.; Marras, S.; Locardi, F.; Nelli, I.; Ferretti, M.; Prato, M.; Manna, L. Postsynthesis Transformation of Insulating Cs4PbBr6 Nanocrystals into Bright Perovskite $CsPbBr_3$ through Physical and Chemical Extraction of CsBr. *ACS Energy Letters* **2017**, *2*, 2445−2448.
(51) de Weerd, C.; Lin, J.; Gomez, L.; Fujiwara, Y.; Suenaga, K.; Gregorkiewicz, T. Hybridization of Single Nanocrystals of Cs_4PbBr_6 and $CsPbBr_3$. *J. Phys. Chem. C* **2017**, *121*, 19490−19496.
(52) Huang, H.; Susha, A. S.; Kershaw, S. V.; Hung, T. F.; Rogach, A. L. Control of Emission Color of High Quantum Yield CH3NH3PbBr3 Perovskite Quantum Dots by Precipitation Temperature. *Adv. Sci. (Weinh)* **2015**, *2*, 1500194.
(53) Sun, S.; Yuan, D.; Xu, Y.; Wang, A.; Deng, Z. Ligand-Mediated Synthesis of Shape-Controlled Cesium Lead Halide Perovskite Nanocrystals via Reprecipitation Process at Room Temperature. *ACS Nano* **2016**, *10*, 3648−3657.
(54) Zhang, Z. Y.; Wang, H. Y.; Zhang, Y. X.; Hao, Y. W.; Sun, C.; Zhang, Y.; Gao, B. R.; Chen, Q. D.; Sun, H. B. The Role of Trap-assisted Recombination in Luminescent Properties of Organometal Halide $CH_3NH_3PbBr_3$ Perovskite Films and Quantum Dots. *Sci. Rep.* **2016**, *6*, 27286.
(55) Yang, G.-L.; Zhong, H.-Z. Organometal halide perovskite quantum dots: synthesis, optical properties, and display applications. *Chin. Chem. Lett.* **2016**, *27*, 1124−1130.
(56) Seth, S.; Samanta, A. Fluorescent Phase-Pure Zero-Dimensional Perovskite-Related Cs_4PbBr_6 Microdisks: Synthesis and Single-Particle Imaging Study. *J. Phys. Chem. Lett.* **2017**, *8*, 4461−4467.
(57) Saidaminov, M. I.; Almutlaq, J.; Sarmah, S.; Dursun, I.; Zhumekenov, A. A.; Begum, R.; Pan, J.; Cho, N.; Mohammed, O. F.; Bakr, O. M. Pure Cs_4PbBr_6: Highly Luminescent Zero-Dimensional Perovskite Solids. *ACS Energy Letters* **2016**, *1*, 840−845.
(58) Koolyk, M.; Amgar, D.; Aharon, S.; Etgar, L. Kinetics of cesium lead halide perovskite nanoparticle growth; focusing and de-focusing of size distribution. *Nanoscale* **2016**, *8*, 6403−6409.

DOI: 10.1021/acs.jpcc.8b02499
J. Phys. Chem. C XXXX, XXX, XXX−XXX

(59) Ha, S.-T.; Su, R.; Xing, J.; Zhang, Q.; Xiong, Q. Metal halide perovskite nanomaterials: synthesis and applications. *Chemical Science* **2017**, *8*, 2522−2536.
(60) Cho, H.; Jeong, S. H.; Park, M. H.; Kim, Y. H.; Wolf, C.; Lee, C. L.; Heo, J. H.; Sadhanala, A.; Myoung, N.; Yoo, S.; et al. Overcoming the electroluminescence efficiency limitations of perovskite light-emitting diodes. *Science* **2015**, *350*, 1222−1225.
(61) Zhang, F.; Zhong, H.; Chen, C.; Wu, X. G.; Hu, X.; Huang, H.; Han, J.; Zou, B.; Dong, Y. Brightly Luminescent and Color-Tunable Colloidal $CH_3NH_3PbX_3$ (X = Br, I, Cl) Quantum Dots: Potential Alternatives for Display Technology. *ACS Nano* **2015**, *9*, 4533−4542.
(62) Li, X.; Wu, Y.; Zhang, S.; Cai, B.; Gu, Y.; Song, J.; Zeng, H. $CsPbX_3$ Quantum Dots for Lighting and Displays: Room-Temperature Synthesis, Photoluminescence Superiorities, Underlying Origins and White Light-Emitting Diodes. *Adv. Funct. Mater.* **2016**, *26*, 2435−2445.
(63) Liu, P.; Chen, W.; Wang, W.; Xu, B.; Wu, D.; Hao, J.; Cao, W.; Fang, F.; Li, Y.; Zeng, Y.; et al. Halide-Rich Synthesized Cesium Lead Bromide Perovskite Nanocrystals for Light-Emitting Diodes with Improved Performance. *Chem. Mater.* **2017**, *29*, 5168−5173.
(64) Kovalenko, M. V.; Protesescu, L.; Bodnarchuk, M. I. Properties and potential optoelectronic applications of lead halide perovskite nanocrystals. *Science* **2017**, *358*, 745−750.
(65) Whittles, T. J.; Burton, L. A.; Skelton, J. M.; Walsh, A.; Veal, T. D.; Dhanak, V. R. Band Alignments, Valence Bands, and Core Levels in the Tin Sulfides SnS, SnS_2, and Sn_2S_3: Experiment and Theory. *Chem. Mater.* **2016**, *28*, 3718−3726.
(66) Wang, A.; Yan, X.; Zhang, M.; Sun, S.; Yang, M.; Shen, W.; Pan, X.; Wang, P.; Deng, Z. Controlled Synthesis of Lead-Free and Stable Perovskite Derivative Cs_2SnI_6 Nanocrystals via a Facile Hot-Injection Process. *Chem. Mater.* **2016**, *28*, 8132−8140.
(67) Swarnkar, A.; Mir, W. J.; Nag, A. Can B-Site Doping or Alloying Improve Thermal- and Phase-Stability of All-Inorganic $CsPbX_3$ (X = Cl, Br, I) Perovskites? *ACS Energy Letters* **2018**, *3*, 286−289.

DOI: 10.1021/acs.jpcc.8b02499
J. Phys. Chem. C XXXX, XXX, XXX−XXX